Magnetoplasmons in lateral multiwire superlattices

1999 J. Phys.: Condens. Matter 11 4199

(http://iopscience.iop.org/0953-8984/11/21/308)

J. Phys.: Condens. Matter **11** (1999) 4199–4217. Printed in the UK PII: S0953-8984(99)99816-8

Magnetoplasmons in lateral multiwire superlattices

L Wendler† and V G Grigoryan‡

† Anna-Siemsen-Straße 66, D-07745 Jena, Germany

‡ Altenberger Straße 48, D-01277 Dresden, Germany

Received 1 December 1998

Abstract. We present a quantum theory of magnetoplasmons in lateral multiwire superlattices. The calculation of the dynamical response is performed in the framework of the random-phase approximation using the tight-binding approximation for the electronic ground state. The dependences of the dispersion relations of the magnetoplasmons on the propagation direction, magnetic field and period of the lateral multiwire superlattice are investigated in detail. It is shown that the magnetoplasmon spectrum shows fine-structure effects. Special attention is directed to the strong-confinement case, where the size-quantization effects in each wire are most important and electron tunnelling between the wires is weak.

1. Introduction

The progress in epitaxial crystal growth techniques of the last decade, which made it possible to fabricate layered semiconductor heterostructures precise on the atomic scale, initiated a broad range of fundamental research and novel applications in many fields of semiconductor physics. These novel devices have unique physical properties, which arise from the *quasi-two-dimensional* (Q2D) behaviour of the carriers. One of the challenging topics of current interest involves systems of further reduced dimensionality: Q1D *quantum-well wires* (QWWs), Q0D *quantum dots* (QDs) and *quantum rings* (QRs). Quantum confinement caused by an artificial spatially varying potential in the growth direction and in one lateral direction is realized in a QWW, where the electron dynamics is essentially restricted to being quasi-one-dimensional. Such QWWs with thicknesses less than 10 nm in the growth direction and lateral widths smaller than 400 nm have been fabricated [1–5].

The spectrum of the collective charge-density excitations, i.e. of *plasmons*, characteristically depends on the dimensionality of the systems. Q1D plasmons have been explored theoretically for isolated QWWs and *lateral multiwire superlattices* (LMWSLs) (see e.g. [6–31]). Most of the theoretical work was done on a quantum-mechanical level using the *random-phase approximation* (RPA) to calculate the linear response to an external charge neglecting retardation and within the hydrodynamic model, which is a phenomenological model. The theoretical work on Q1D plasmons predicts, according to the size quantization, two different types of excitations: *intrasubband plasmons*, which are connected with collective (coherent) electron motion within one electric subband, and *intersubband plasmons*, which are connected with collective (coherent) electron motion between two different electric subbands.

The excitation spectrum of the *quasi-one-dimensional electron gas* (Q1DEG) has been studied experimentally by *far-infrared* (FIR) *optical absorption* (see e.g. [4, 5, 32–36]) and *inelastic light scattering* (see e.g. [3,37–44]). Most of the FIR optical measurements performed up to now study the *collective intersubband transitions* (*intersubband resonances, dimensional*

0953-8984/99/214199+19$19.50

resonances), which are associated with the collective electronic motion between different subbands and which are standing waves in the lateral direction of the QWW. Plasmons, which are travelling waves along the wire axis, are excited in FIR transmission with the help of a metallic grating coupler on top of the sample. In contrast, in inelastic light scattering experiments it is possible to observe plasmons directly.

The effects of a quantizing magnetic field on intra- and intersubband plasmons in single QWWs are investigated extensively. FIR optical transmission experiments on QWWs with an applied external magnetic field show a more complex resonance structure than in the absence of the magnetic field. Unfortunately, earlier theories on magnetoplasmons [9, 18] fail to explain these experimental findings and give quite different results for the Q1D magnetoplasmons.

Recently, the authors of the present paper presented a new quantum-mechanical approach for investigating the dynamical properties of the Q1DEG, quantum confined in a single isolated QWW, in the presence of a static magnetic field [29–31]. Using this fully non-local RPA response theory it was shown that *additional* intersubband magnetoplasmons exist in comparison to (i) a Q1DEG in the absence of a magnetic field and to (ii) a (strict) 2DEG (i.e. a Q2DEG of zero thickness) in the presence of a static magnetic field. For large magnetic fields the dispersion curve of the intrasubband plasmon (there is only one if one subband is occupied) tends to zero like an edge magnetoplasmon of a spatially confined 2DEG, whereas the intersubband magnetoplasmons have dispersion relations approaching the frequencies of the *principal* and *Bernstein* modes of a 2DEG in this limit. On the basis of these results it is possible to interpret the Q1D magnetoplasmons in the range of larger magnetic fields as *size-quantized (confined)* principal and Bernstein modes. But in contrast to the case for the 2DEG, for the Q1DEG more than one branch of dispersion curves approaches each asymptote. The *additional modes* (AMs) arise due to the reduced symmetry of the system, i.e. the spectrum of the Q1D magnetoplasmons shows *fine-structure effects* [29–31]. At smaller magnetic fields all the modes strongly hybridize and the spectrum of the Q1D magnetoplasmons results. For $B \to 0$ the AMs approach the frequencies of the single-particle excitations and, thus, lose their collective character analogously to the Bernstein modes of higher-dimensional electron gases in this limit. Thus, at small magnetic fields the AMs of a single isolated QWW may be interpreted as the Q1D analogues of the Bernstein modes. The remaining dispersion curves approach at $B = 0$ the frequencies of the Q1D plasmons and, hence, are called *fundamental modes* (FMs). It is shown that this physical picture of the mode spectrum is *universal*, i.e. does not depend on the concrete shape of the lateral confining potential. Furthermore, it is shown [45] that the Q1DEG in a single QWW absorbs normally incident FIR light at the frequencies of the antisymmetric intersubband resonances of both FMs and AMs. Whereas the antisymmetric FMs absorb the light with a strength which increases with increasing magnetic field, the absorption strength of the antisymmetric AMs vanishes for zero and very large magnetic fields.

However, up to now the theory of magnetoplasmons of LMWSLs has attracted only little attention. This is somewhat surprising because most experiments are performed on LMWSLs and not on single QWWs. LMWSLs can be made, for example, by fabricating using nanotechniques a grating-like gate on top of a semiconductor heterostructure containing a Q2DEG. If a gate voltage is applied, a periodic electron-density modulation is induced via the field effect in the Q2DEG, which can be tuned up to the periodic array of parallel QWWs, schematically shown in figure 1. Electrons move freely along the wire axes, but experience a periodic confining potential in the direction perpendicular to the wires. Three important effects are present for collective excitations in LMWSLs: (i) size quantization in each wire in the lateral direction, (ii) tunnelling of the electrons between the wires and (iii) Coulomb coupling between the electrons of different wires.

In the present paper we extend our previous work on Q1D magnetoplasmons in single

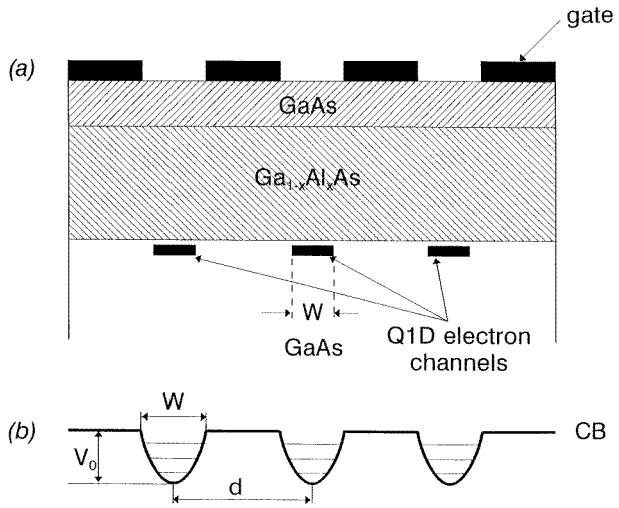

Figure 1. A schematic representation of a lateral multiwire superlattice induced via the field effect of a grating-like gate on top of the sample (a). The lower part (b) schematically shows the spatial dependence of the conduction-band edge and the subband quantization in each single QWW. The effective widths of the single-electron channels are w, V_0 is the depth of the single-well parabolic potential and d is the superlattice period.

QWWs [29–31] to LMWSLs. The aim of this paper is to develop a theory of the density response for a LMWSL in the presence of a quantizing magnetic field and to find an answer to the question regarding the influence of the lateral periodicity and interwire Coulomb interaction on the properties of the magnetoplasmon spectrum, especially on its fine structure.

The present paper is arranged as follows. In section 2 the electronic ground state is considered. The density response of the LMWSL in the presence of an externally applied magnetic field is developed in section 3. In section 4 we present the numerical results for the dispersion relations of the magnetoplasmons in LMWSLs and we give our conclusions in section 5.

2. Ground state

The electrons present in the different laterally arranged wires forming the LMWSL couple through the Coulomb interaction and the electron wave functions may overlap in the lateral direction, thereby giving rise to possible lateral electron tunnelling between adjacent QWWs. This overlap of the electron wave functions we will treat in the *tight-binding approximation*. The unperturbed effective single-particle Hamiltonian in the effective-mass approximation for the electrons of the LMWSL in the presence of a static homogeneous magnetic field $\boldsymbol{B} = (0, 0, B)$, applied perpendicular to the heterointerfaces, is given by

$$H_0 = \frac{1}{2m_e}[\boldsymbol{p}_e + e\boldsymbol{A}(\boldsymbol{x})]^2 + V_{eff}(\boldsymbol{x})$$

where we ignore the Zeeman spin splitting. Throughout this paper we omit the spin quantum number and coordinate, but assume that the spin summation is included when necessary without any explicit indication. Here, $\boldsymbol{p}_e = (\hbar/\mathrm{i})\boldsymbol{\nabla}$ is the momentum operator of the electron with charge $-e$ and effective conduction-band-edge mass m_e and $\boldsymbol{A}(\boldsymbol{x})$ is the vector potential of the (externally applied) DC magnetic field $\boldsymbol{B} = \boldsymbol{\nabla} \times \boldsymbol{A}(\boldsymbol{x})$. The *effective confining potential*

$V_{eff}(\boldsymbol{x}) = V_{eff}(y, z)$ is the sum of the *bare potential* and the many-particle contributions (*Hartree potential* and *exchange–correlation potential*) and gives rise to electron confinement in two spatial directions, which we choose to be the y-direction (lateral direction) and the z-direction (growth direction). In the x-direction, along the wire axes, the electron motion is assumed to be quasi-free. Self-consistent calculations [46] reveal that the separation

$$V_{eff}(y, z) = V_{eff}(y) + V_{eff}(z)$$

is reasonable as long as the confinement in the lateral direction is much weaker than that in the growth direction. This is the case in the experimentally realized systems, considered in this paper. Here, we assume for simplicity, but without loss of generality, that $V_{eff}(z)$ confines the electrons in a zero-thickness x–y plane at $z = 0$. In the y-direction the potential is periodic:

$$V_{eff}(y) = V_{eff}(y + md)$$

with d the *superlattice period*. In this direction we assume Born–von Kármán boundary conditions and $m = 0, 1, 2, \ldots, M-1$ wells within the unit length $L_y = Md$. The effective confining potential in the y-direction is assumed to be constructed in the form

$$V_{eff}(y) = \sum_{m=0}^{M-1} V_{eff}^{sw}(y - md)$$

where $V_{eff}^{sw}(y - md)$ is the effective potential of a single well centred at $y = md$.

One suitable example for the single-well potential, which usually appears in semiconductor nanostructures with electrostatic confinement and small electron densities, is a parabolic potential of finite height V_0:

$$V_{eff}^{sw}(y - md) = \begin{cases} m_e\Omega^2(y - md)^2/2 & \text{if } |y - md| \leqslant w/2 \\ V_0 & \text{otherwise} \end{cases}$$

where $w = [8V_0/(m_e\Omega^2)]^{1/2}$ is the width of the well and Ω is the confining frequency. Such a shape of the effective potential is justified by self-consistent ground-state calculations [47]. With the use of the Landau gauge $\boldsymbol{A}(\boldsymbol{x}) = (-yB, 0, 0)$ for the vector potential the single-particle Hamiltonian of a single parabolic well at $y = md$ reads

$$H_0^{sw} = \begin{cases} \dfrac{\boldsymbol{p}_e^2}{2m_e} - \omega_c(y - md)p_{e_x} + \dfrac{m_e}{2}\tilde{\omega}_c^2(y - md)^2 + V_{eff}(z) & \text{if } |y - md| \leqslant \dfrac{w}{2} \\ \dfrac{\boldsymbol{p}_e^2}{2m_e} - \omega_c y p_{e_x} + \dfrac{m_e}{2}\omega_c^2 y^2 + V_0 + V_{eff}(z) & \text{if } |y - md| > \dfrac{w}{2} \end{cases} \tag{1}$$

where p_{e_α} is the αth component of the electron momentum operator, $\omega_c = eB/m_e$ is the cyclotron frequency and $\tilde{\omega}_c = (\omega_c^2 + \Omega^2)^{1/2}$ is the hybrid frequency. Because $[p_{e_x}, H_0^{sw}] = 0$, one can diagonalize p_{e_x} and H_0^{sw} simultaneously. For each eigenvalue $\hbar k_x$ of p_{e_x} (k_x is the electron wave-vector component in the x-direction), the Hamiltonian has a discrete spectrum of energy eigenvalues, resulting from the electron motion in the y- and z-directions. Thus, the eigenvalue problem of H_0^{sw} in the y–z plane becomes equivalent to two separate equations, one for the size quantization in the z-direction and one for the mixed size and magnetic quantization in the y-direction. The single-particle Schrödinger equation for the electron motion in the single well at $z = md$ is solved by the wave function

$$\langle \boldsymbol{x}|N, k_x\rangle^{sw} \equiv \Psi_{Nk_x}^{sw}(\boldsymbol{x}) = \frac{1}{\sqrt{L_x}} \mathrm{e}^{\mathrm{i}k_x x} \Phi_N(y - Y_{k_x} - md)\varphi(z) \tag{2}$$

where L_x is the unit length in the x-direction (we assume Born–von Kármán boundary conditions). Furthermore, $Y_{k_x} = \gamma \tilde{l}_0^2 k_x$ is the centre coordinate with $\tilde{l}_0 = [\hbar/(m_e\tilde{\omega}_c)]^{1/2}$ the

effective width of the wave function in the y-direction and we have defined $\gamma = \omega_c/\tilde{\omega}_c$ and $|\varphi(z)|^2 = \delta(z)$. In general, the wave function $\Phi_N(y - Y_{k_x} - md)$ of a single electron inside a single parabolic quantum well of finite height is given by a degenerate hypergeometric function and for motion outside by an exponential function. Fortunately, under the condition $\overline{h}\Omega/V_0 \ll 1$, for the energetically lowest-lying levels, this wave function can be approximated by the shifted harmonic-oscillator wave function:

$$\Phi_N(y - Y_{k_x} - md) = \frac{1}{\sqrt{2^N N!\pi^{1/2}\tilde{l}_0}} \exp\left[-\frac{1}{2\tilde{l}_0^2}(y - Y_{k_x} - md)^2\right] \times H_N\left[\frac{1}{\tilde{l}_0}(y - Y_{k_x} - md)\right] \tag{3}$$

where $H_N(y)$ is Hermite's polynomial. The associated energy eigenvalues of this single QWW follow in the well-known form $\mathcal{E}_N(k_x) = \mathcal{E}_N + \overline{h}^2 k_x^2/(2\tilde{m}_e)$, where in this case the subband bottoms are given by $\mathcal{E}_N = \overline{h}\tilde{\omega}_c(N + 1/2)$; $N = 0, 1, 2, \ldots$, and $\tilde{m}_e = m_e(\tilde{\omega}_c/\Omega)^2$ is the magnetic-field-dependent effective mass.

The single-particle wave function of the LMWSL is given in the tight-binding approximation by

$$\Psi_{Nk_xk_y}(\boldsymbol{x}) = \frac{1}{\sqrt{L_x}} e^{ik_x x} \eta_{Nk_xk_y}(y - Y_{k_x})\varphi(z) \tag{4}$$

with

$$\eta_{Nk_xk_y}(y - Y_{k_x}) = \sum_{N'=0}^{\infty} \sum_{m=0}^{M-1} C_{NN'}(k_y) e^{ik_y md} \Phi_{N'}(y - Y_{k_x} - md) \tag{5}$$

assuming that the centre coordinate is located inside the associated single QWW. Obviously,

$$\eta_{Nk_xk_y}(y - Y_{k_x} + nd) = e^{ik_y nd} \eta_{Nk_xk_y}(y - Y_{k_x})$$

is fulfilled and, thus, we have

$$\eta_{Nk_xk_y}(y - Y_{k_x}) = e^{ik_y y} u_{Nk_xk_y}(y - Y_{k_x})$$

according to Bloch's theorem with

$$u_{Nk_xk_y}(y - Y_{k_x} + nd) = u_{Nk_xk_y}(y - Y_{k_x}) \equiv \sum_{N'=0}^{\infty} \sum_{m=0}^{M-1} C_{NN'}(k_y) e^{-ik_y(y-md)} \Phi_{N'}(y - Y_{k_x} - md).$$

If the levels of the single well are non-degenerate and well separated, no hybridization takes place, i.e. we have $C_{NN'}(k_y) = \delta_{NN'} C_{Nk_y}/\sqrt{M}$, where

$$C_{Nk_y} = \frac{1}{\sqrt{1 + 2\alpha_N \cos(k_y d)}}. \tag{6}$$

Herein, α_N is the nearest-neighbour overlap parameter

$$\alpha_N = \int_{-d/2}^{3d/2} dy\ \Phi_N^*(y)\Phi_N(y - d). \tag{7}$$

The associated energy eigenvalues of a single electron in the LMWSL, the *minibands*, are given by

$$\mathcal{E}_N(k_x, k_y) = \mathcal{E}_N + \beta_{Nk_x}[1 - 2\alpha_N \cos(k_y d)] + 2\gamma_{Nk_x} \cos(k_y d) + \frac{\overline{h}^2 k_x^2}{2\tilde{m}_e} \tag{8}$$

where

$$\beta_{Nk_x} = \int_{-d/2}^{d/2} \mathrm{d}y\ \Phi_N^*(y - Y_{k_x})\,\Delta V_{eff}(y)\,\Phi_N(y - Y_{k_x}) \tag{9}$$

$$\gamma_{Nk_x} = \int_{-d/2}^{3d/2} \mathrm{d}y\ \Phi_N^*(y - Y_{k_x})\,\Delta V_{eff}(y)\,\Phi_N(y - Y_{k_x} - d) \tag{10}$$

and $\Delta V_{eff}(y) = V_{eff}(y) - V_{eff}^{sw}(y)$. For a superlattice potential of the form

$$V_{eff}(y) = \sum_{m=0}^{M-1} V_{eff}^{sw}(y - md)$$

under consideration, we have $\Delta V_{eff}(y) = 0$ for $-d/2 \leqslant y \leqslant d/2$ and, thus, $\beta_{Nk_x} = 0$. It becomes obvious that $\mathcal{E}_N(k_x, k_y) = \mathcal{E}_N(k_x, k_y + G_n)$ is valid, where $G_n = (2\pi/d)n$; $n = 0, \pm 1, \pm 2, \ldots$, is the *reciprocal-lattice vector* of the LMWSL and, thus, the wave-vector component k_y varies within the *first mini-Brillouin zone* $-\pi/d < k_y \leqslant \pi/d$.

The Fermi energy E_F is obtained from the self-consistently solved equation

$$n_{2DEG} = \frac{1}{2\pi^2} \sum_N \int_{-\infty}^{\infty} \mathrm{d}k_x \int_{-\pi/d}^{\pi/d} \mathrm{d}k_y\ \Theta\left(E_F - \mathcal{E}_N - 2\gamma_{Nk_x}\cos(k_y d) - \frac{\hbar^2 k_x^2}{2\tilde{m}_e}\right) \tag{11}$$

where n_{2DEG} is the number of electrons per unit area $A = L_x L_y$. In the absence of tunnelling we have $\gamma_{Nk_x} = 0$ and from equation (11) it follows that

$$n_{1DEG} = \frac{4}{\pi\hbar}\sqrt{\frac{\tilde{m}_e}{2}} \sum_N \sqrt{E_F - \mathcal{E}_N}\,\Theta(E_F - \mathcal{E}_N). \tag{12}$$

Herein, $n_{1DEG} = n_{2DEG}d$ is the number of electrons per unit length in a single QWW and $\Theta(x)$ is the Heaviside unit step function: $\Theta(x) = 1$ for $x > 1$ and $\Theta(x) = 0$ for $x < 0$.

3. Density response of a LMWSL

In this section, we calculate the linear response of a LMWSL to an external (scalar) potential on a quantum-mechanical level in the framework of the RPA, using the *self-consistent-field* (SCF) method. For many purposes, 1D systems are simpler than 3D ones, because the more restricted phase space often allows one to obtain exact solutions to non-trivial statistical-mechanical problems. Unfortunately, this situation does not apply to problems involving electrodynamics. Because of the three-dimensionality of the sample, the fields are not only in the Q1D electron channel but also in the surrounding media. As a result of this Coulomb coupling the relations between the quantum-confined charges and the potentials become non-local and very complex and, thus, the different electron motions are not independent.

The single-particle Hamiltonian of the electrons confined in the LMWSL in the presence of the perturbation is written as $H(\boldsymbol{x}, t) = H_0(\boldsymbol{x}) + H_1(\boldsymbol{x}, t)$, where H_0 is the Hamiltonian of the unperturbed system, satisfying the eigenvalue equation

$$H_0|N, k_x, k_y\rangle = \mathcal{E}_N(k_x, k_y)|N, k_x, k_y\rangle$$

and the perturbation $H_1 = V^{sc}(\boldsymbol{x}, t)$ is the *self-consistent potential*, which is a sum of the *external potential* $V^{ext}(\boldsymbol{x}, t)$ and the *induced potential* $V^{ind}(\boldsymbol{x}, t)$. Writing the statistical operator ϱ_G of the system as $\varrho_G = \varrho_G^{(0)} + \varrho_G^{(1)}$, where $\varrho_G^{(0)}$ is the single-particle statistical operator of the unperturbed system and $\varrho_G^{(1)}$ is the correction to the statistical operator to the

first order in the perturbation, switching on the external potential adiabatically and taking matrix elements of the linearized von Neumann equation, it follows that

$$\langle N, k_x, k_y|\varrho_G^{(1)}|N', k_x', k_y'\rangle = \frac{n_F[\mathcal{E}_{N'}(k_x', k_y')] - n_F[\mathcal{E}_N(k_x, k_y)]}{\hbar(\omega + \mathrm{i}\delta) + \mathcal{E}_{N'}(k_x', k_y') - \mathcal{E}_N(k_x, k_y)} \langle N, k_x, k_y|V^{sc}(\boldsymbol{x}, \omega)|N', k_x', k_y'\rangle. \quad (13)$$

In this equation,

$$\varrho_G^{(0)}|N, k_x, k_y\rangle = n_F[\mathcal{E}_N(k_x, k_y)]|N, k_x, k_y\rangle$$

is used, with $n_F[\mathcal{E}_N(k_x, k_y)] = \Theta[E_F - \mathcal{E}_N(k_x, k_y)]$ the Fermi distribution function at $T = 0$ and $\delta \to 0^+$. Next, we calculate the (frequency-dependent) total electron number density $n(\boldsymbol{x}, \omega) = n_0(\boldsymbol{x}) + n_{ind}(\boldsymbol{x}, \omega)$ of the LMWSL, which is a sum of the equilibrium ground-state electron number density $n_0(\boldsymbol{x}) = \mathrm{Tr}\,\{\varrho_G^{(0)}\delta(\boldsymbol{x} - \boldsymbol{x}_e)\}$ and the induced electron number density $n_{ind}(\boldsymbol{x}, \omega) = \mathrm{Tr}\,\{\varrho_G^{(1)}\delta(\boldsymbol{x} - \boldsymbol{x}_e)\}$, performing the trace (Tr) in the grand-canonical ensemble. According to the translational invariance in the x-direction (homogeneity), the x-component q_x of the wave vector is a conserved quantity. However, in the y-direction the translational symmetry (periodicity) guarantees that the y-component of the wave vector q_y is conserved only up to the reciprocal-lattice vector G_n. This means that a perturbation of the wave-vector component q_y induces a response at all wave vectors $q_y + G_n$, where G_n is any reciprocal-lattice vector. This symmetry property is profitable exploited by using the 2D Fourier (series) transform

$$f(\boldsymbol{x}, \omega) = \frac{1}{L_x L_y} \sum_{q_x} \sum_{\substack{q_y \\ (q_y \in \text{first mBz})}} \sum_{G_n} \mathrm{e}^{\mathrm{i}q_x x} \mathrm{e}^{\mathrm{i}(q_y + G_n)y} f(q_x, q_y + G_n; z|\omega) \quad (14)$$

and its inverse

$$f(q_x, q_y + G_n; z|\omega) = \int_{L_x} \mathrm{d}x \int_{L_y} \mathrm{d}y\, \mathrm{e}^{-\mathrm{i}q_x x} \mathrm{e}^{-\mathrm{i}(q_y + G_n)y} f(\boldsymbol{x}, \omega) \quad (15)$$

where the sum over q_y extends over all values in the first mini-Brillouin zone (mBz). Then, the density response $n_{ind}(q_x, q_y + G_n; z|\omega)$ to $V^{sc}(q_x, q_y + G_n; z|\omega)$ is given by

$$n_{ind}(q_x, q_y + G_n; z|\omega) = \sum_{G_n'} P^{(1)}(q_x, q_y + G_n, q_y + G_n'|\omega) V^{sc}(q_x, q_y + G_n'; z|\omega)\delta(z) \quad (16)$$

where $P^{(1)}(q_x, q_y + G_n, q_y + G_n'|\omega)$ is the *irreducible* RPA *polarization function*,

$$P^{(1)}(q_x, q_y + G_n, q_y + G_n'|\omega) = \sum_{NN'} P_{NN'}^{(1)}(q_x, q_y + G_n, q_y + G_n'|\omega) \quad (17)$$

and the *matrix polarization function* $P_{NN'}^{(1)}(q_x, q_y + G_n, q_y + G_n'|\omega)$ reads

$$P_{NN'}^{(1)}(q_x, q_y + G_n, q_y + G_n'|\omega) = \frac{2}{L_x L_y} \sum_{k_x} \sum_{\substack{k_y \\ (k_y \in \text{first mBz})}} \frac{n_F[\mathcal{E}_{N'}(k_x + q_x, k_y - q_y)] - n_F[\mathcal{E}_N(k_x, k_y)]}{\hbar(\omega + \mathrm{i}\delta) + \mathcal{E}_{N'}(k_x + q_x, k_y - q_y) - \mathcal{E}_N(k_x, k_y)} \times |C_{Nk_y} C_{N'k_y - q_y}|^2 B_{NN'}(k_x, k_y, q_x, q_y + G_n) B_{NN'}^*(k_x, k_y, q_x, q_y + G_n') \quad (18)$$

where

$$B_{NN'}(k_x, k_y, q_x, q_y + G_n) = \sum_{m=0}^{M-1} \mathrm{e}^{\mathrm{i}k_y md} A_{NN'}^{(m)}(k_x, q_x, q_y + G_n) \quad (19)$$

with

$$A^{(m)}_{NN'}(k_x, q_x, q_y + G_n) = \int_0^{L_y} \mathrm{d}y\, \mathrm{e}^{\mathrm{i}(q_y+G_n)y} \Phi^*_N(y - Y_{k_x} - md)\Phi_{N'}(y - Y_{k_x+q_x}). \tag{20}$$

For the model of the LMWSL chosen here we obtain

$$\begin{aligned} A^{(m)}_{NN'}(k_x, q_x, q_y + G_n) = {} & \left(\frac{L_2!}{2^{L_1-L_2}L_1!}\right)^{1/2} \exp\left\{-\frac{1}{4}\left[(q_y + G_n)^2\tilde{l}_0^2 + \left(\gamma\tilde{l}_0 q_x + \frac{md}{\tilde{l}_0}\right)^2\right]\right. \\ & \left. + \mathrm{i}\frac{(q_y + G_n)\tilde{l}_0}{2}\left[\gamma\tilde{l}_0(2k_x + q_x) - \frac{md}{\tilde{l}_0}\right]\right\} \\ & \times \left[\mathrm{i}(q_y + G_n)\tilde{l}_0 - \mathrm{sgn}(N' - N)\left(\gamma\tilde{l}_0 q_x + \frac{md}{\tilde{l}_0}\right)\right]^{N_1-N_2} \\ & \times L_{N_2}^{N_1-N_2}\left\{\frac{1}{2}\left[(q_y + G_n)^2\tilde{l}_0^2 + \left(\gamma\tilde{l}_0 q_x + \frac{md}{\tilde{l}_0}\right)^2\right]\right\} \end{aligned} \tag{21}$$

where $N_1 = \max(N, N')$, $N_2 = \min(N, N')$, $L_N^{N'}(x)$ is the associated Laguerre polynomial and we have defined $\mathrm{sgn}(x) = +1$ for $x \geqslant 0$ and $\mathrm{sgn}(x) = -1$ for $x < 0$.

The induced density is the source of the induced potential. In the RPA and neglecting retardation effects (the influence of retardation effects is discussed e.g. in reference [24]) both quantities are related via Poisson's equation. Assuming a homogeneous dielectric background, i.e. we neglect image effects (the influence of image effects is discussed e.g. in references [25, 27]), Poisson's equation reads

$$\left[\frac{\partial^2}{\partial z^2} - [q_x^2 + (q_y + G_n)^2]\right] V^{ind}(q_x, q_y + G_n; z|\omega) = -\frac{e^2}{\varepsilon_0\varepsilon_s} n_{ind}(q_x, q_y + G_n; z|\omega) \tag{22}$$

where ε_0 is the permittivity of vacuum. For the screening of the homogeneous dielectric background we use the ε_s-approximation, i.e. use the static electric constant ε_s. The self-consistent potential follows from equation (22) in the form

$$\begin{aligned} V^{sc}(q_x, q_y + G_n; z|\omega) = {} & V^{ext}(q_x, q_y + G_n, z|\omega) + V^s(q_x, q_y + G_n)\mathrm{e}^{-\sqrt{q_x^2+(q_y+G_n)^2}|z|} \\ & \times \sum_{G'_n} P^{(1)}(q_x, q_y + G_n, q_y + G'_n|\omega) V^{sc}(q_x, q_y + G'_n; 0|\omega) \end{aligned} \tag{23}$$

where

$$V^s(q_x, q_y + G_n) = \frac{e^2}{2\varepsilon_0\varepsilon_s\sqrt{q_x^2 + (q_y + G_n)^2}}. \tag{24}$$

Taking the matrix elements of equation (23) with the wave functions of equation (4) and assuming that collective charge-density excitations of the LMWSL exist under the condition that $V^{sc} \neq 0$ while $V^{ext} = 0$, the existence condition for the collective excitation reads

$$\det\left[\delta_{G_nG'_n} - V^s(q_x, q_y + G_n)P^{(1)}(q_x, q_y + G_n, q_y + G'_n|\omega)\right] = 0. \tag{25}$$

This determinantal equation is the *dispersion relation of magnetoplasmons* of LMWSLs if the imaginary part of $P^{(1)}(q_x, q_y + G_n, q_y + G'_n|\omega)$ is zero. In the dispersion relation all minibands $\mathcal{E}_N(k_x, k_y)$ are involved in the RPA polarization function, equation (17). Then, due to the *intersubband (or interminiband) coupling* (ISC) the collective motion of the electrons is not independent in and between the different minibands. Thus, a magnetoplasmon excited in the LMWSL is in principle accompanied by all possible electron motions: (i) within the occupied minibands and (ii) between the different minibands. Which collective intra- and interminiband motions are coupled in a definite situation depends on the symmetry properties of the sample

under consideration (see e.g. the discussion in reference [31]). Only in the absence of ISC, do '*pure*' $(N–N)$ *intrasubband magnetoplasmons*, $\omega = \omega_{mp}^{NN}(q_x, q_y; B)$, accompanied by electron transitions within the miniband N, and do '*pure*' $(N–N')$ *intersubband magnetoplasmons*, $\omega = \omega_{mp}^{NN'}(q_x, q_y; B)$, accompanied by electron transitions between the minibands N' and N, occur. Because usually only a few minibands are occupied, one can successfully apply a *multi-miniband model* with $N = 0, 1, 2, \ldots, \bar{M} - 1$ minibands taken into account. The restriction to a small number of minibands is possible because the matrix polarization function has the properties $P_{NN'}^{(1)}(q_x, q_y + G_n, q_y + G_n'|\omega) \to 0$ if $|N - N'|$ becomes large and $P_{NN'}^{(1)}(q_x, q_y+G_n, q_y+G_n'|\omega) = 0$ if both of the inequalities $\mathcal{E}_N > E_F$ and $\mathcal{E}_N' > E_F$ are fulfilled. It becomes obvious that the dispersion relation, equation (25), depends on Umklapp processes. Because n and n' run through all integers, the determinantal equation is, in principle, of infinite order. For practical purposes, one has to find out how fast the solutions of this determinantal equation converge as a function of G_n and G_n' and choose the order of the determinant on the basis of a suitable convergence criterion.

The dispersion relation of the magnetoplasmons of the LMWSL is very general, valid as long as the tight-binding approximation and the RPA are valid. It is applicable to LMWSLs either with or without electron tunnelling between the wires. In the special situation for which the electron tunnelling between the single QWWs of the LMWSL can be neglected, i.e. if $\bar{h}\Omega / V_0 \ll 1$, we have $B_{NN'}(k_x, k_y, q_x, q_y+G_n) = A_{NN'}^{(0)}(k_x, q_x, q_y+G_n)$ and $C_{Lk_y} = 1$. In this case the collective electron motion in the different wires is coupled via the Coulomb potential (interwire Coulomb interaction), i.e. we have pure *Coulomb-coupled Q1D magnetoplasmons*. This regime is the situation mostly realized in the experiments with which we deal in detail in the next section.

4. Collective excitation: magnetoplasmons of LMWSLs

In this section we present numerical results for the dispersion relations of magnetoplasmons in LMWSLs. Because in the LMWSLs used up to now in experiments the superlattice period d is larger than 150 nm, tunnelling of the electrons between the QWWs is physically unimportant. Thus, we neglect tunnelling in the numerical calculation of the dispersion relations of the collective charge-density excitations. We perform these calculations assuming a three-miniband model. We have chosen a GaAs–$Ga_{1-x}Al_xAs$ LMWSL (GaAs: $\varepsilon_s = 12.87$ and $m_e = 0.06624m_0$; m_0: bare electron mass) with a confining energy $\bar{h}\Omega = 2$ meV of the effective potential $V_{eff}^{sw}(y)$ of a single well and assumed an electron density of $n_{1DEG} = 3 \times 10^5$ cm^{-1}. In this case only the lowest subband of each single QWW is occupied.

The full RPA dispersion relations of the magnetoplasmons of the LMWSL, $\omega = \omega_{mp}^{NN'}(q_x, q_y; B)$, are calculated from equation (25). The dependences of the plasmon dispersion curves $\omega_p^{NN'}(q_x, q_y; B = 0)$ on the wave-vector component q_x for vanishing magnetic field ($B = 0$) and three different periods of the LMWSL are plotted in figure 2. In the case of vanishing magnetic field and $d = 1000$ nm (figure 2(a)) three different branches of dispersion curves of plasmons result for each value of q_y. Because of the large superlattice period the Coulomb coupling is so weak that

$$\omega_p^{NN'}(q_x, q_y = 0; 0) \approx \omega_p^{NN'}(q_x, q_y = \pi/d; 0)$$

i.e. the three branches ω_p^{00}, ω_p^{10} and ω_p^{20} of dispersion curves are nearly identical to that of a single isolated QWW (for details including the notation scheme of the mode used, see references [28, 31]). It is seen from figure 2(a) that the intrasubband plasmon ω_p^{00}

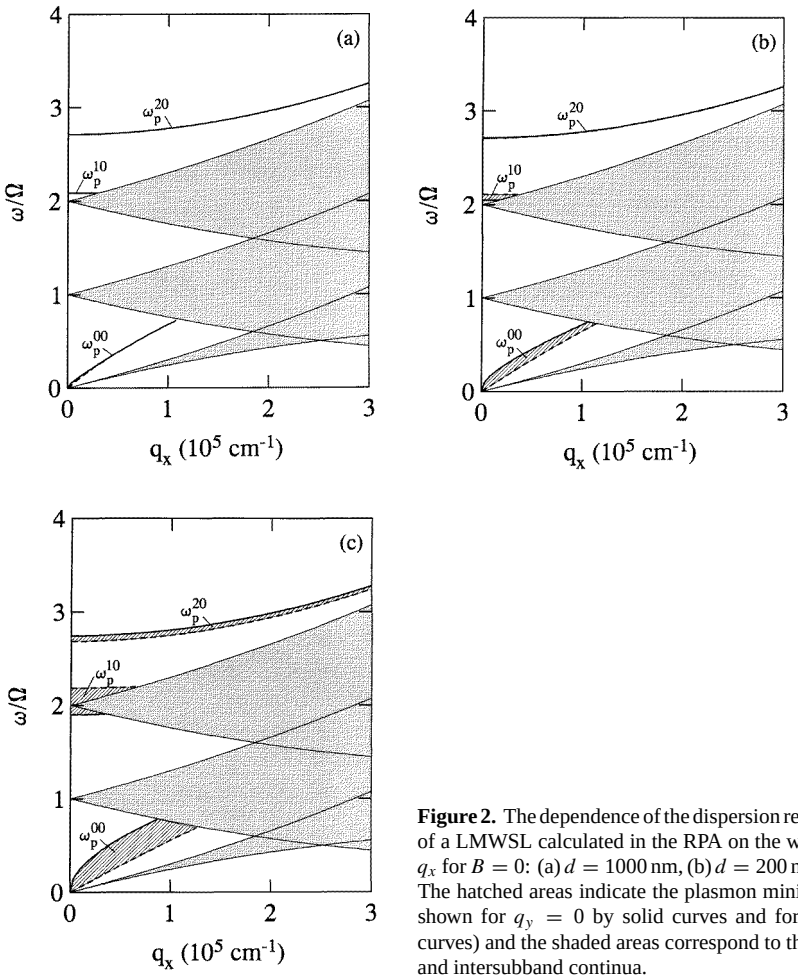

Figure 2. The dependence of the dispersion relations of the plasmons of a LMWSL calculated in the RPA on the wave-vector component q_x for $B = 0$: (a) $d = 1000$ nm, (b) $d = 200$ nm and (c) d = 100 nm. The hatched areas indicate the plasmon minibands (boundaries are shown for $q_y = 0$ by solid curves and for $q_y = \pi/d$ by dashed curves) and the shaded areas correspond to the single-particle intra- and intersubband continua.

has a vanishing frequency for $q_x = 0$, but the intersubband modes ω_p^{10} and ω_p^{20} of the LMWSL start at $q_x = q_y = 0$ above the corresponding subband separation frequency $\Omega_{N0} = (\mathcal{E}_N - \mathcal{E}_0)/\overline{h} = N\Omega$. In the framework of the RPA this frequency shift is the *depolarization shift*

$$\Delta_p^{N0} = \omega_p^{N0}(q_x = 0, q_y = 0; B = 0) - N\Omega.$$

Thus, for large superlattice periods the *long-wavelength dispersion relations* of the lowest frequency Q1D plasmons of the LMWSL are

$$\omega_p^{00}(q_x, q_y; B = 0) \propto q_x l_\Omega \left[\left(\frac{\overline{h}\pi n_{1DEG}}{2m_e l_\Omega} \right)^2 - \frac{n_{1DEG} e^2}{2\pi\varepsilon_0\varepsilon_s m_e l_\Omega} \ln(|q_x| l_\Omega) \right]^{1/2}$$

$$\omega_p^{10}(q_x, q_y; B = 0) \propto \left(1 + \frac{n_{1DEG} e^2}{2\pi\varepsilon_0\varepsilon_s \overline{h}\Omega} \right)^{1/2} \Omega$$

and

$$\omega_p^{20}(q_x, q_y; B = 0) \propto \left(1 + \frac{n_{1DEG} e^2}{8\pi\varepsilon_0\varepsilon_s \overline{h}\Omega} \right)^{1/2} (2\Omega)$$

where $l_\Omega = [\hbar/(m_e\Omega)]^{1/2}$.

The shaded areas in figure 2(a) are the *single-particle continua*, i.e. the regions of existence of the *single-particle excitations* (SPEs). The plasmon dispersion relations are plotted for the LMWSL with $d = 200$ nm and $d = 100$ nm in figures 2(b) and 2(c), respectively. In these and in the following figures we have plotted the different branches ω_p^{00}, ω_p^{10}, ω_p^{20} of dispersion relations for $q_y = 0$ (solid curves) and $q_y = \pi/d$ (dashed curves), i.e. the plotted dispersion curves are the boundaries of the *plasmon and magnetoplasmon minibands*, represented by the differently hatched areas between these curves. This miniband structure of the LMWSL plasmon dispersion relations arises due to the Coulomb coupling between the different wires. It is seen from figures 2(b) and 2(c) that with decreasing superlattice period the difference between $\omega_p^{NN'}(q_x, q_y = 0; 0)$ and $\omega_p^{NN'}(q_x, q_y = \pi/d; 0)$ increases, i.e. the plasmon minibands become broader. Furthermore, it becomes obvious that an increasing of q_y decreases the frequency of the (0–0) intrasubband plasmon branch and that of the (2–0) intersubband plasmon branch, but increases the frequency of the (1–0) intersubband plasmon branch.

The (0–0) intrasubband plasmon branch behaves for smaller superlattice periods and $q_y = 0$ like an *optical plasmon*, i.e. the induced electron densities in adjacent wires oscillate *in phase*. With decreasing d this branch becomes more and more the character of a 2D plasmon: $\omega_p^{00}(q_x, q_y = 0; B = 0) \propto \sqrt{q_x}$. But for $q_y = \frac{\pi}{d}$ the (0–0) intrasubband plasmon branch behaves like an *acoustic plasmon*, i.e. the induced electron densities in adjacent wires oscillate *in anti-phase*. In this case, we have $\omega_p^{00}(q_x, q_y = \frac{\pi}{d}; B = 0) \propto q_x$ for smaller superlattice periods d.

The case of non-vanishing magnetic field ($B = 1$ T) is plotted in figures 3(a) to 3(c). Comparing these figures with figure 2, it becomes obvious that in the presence of a magnetic field additional modes, forming minibands, appear compared to the case $B = 0$. In detail, for the large-period LMWSL (figure 3(a)) we practically reproduce the same dispersion curves as for a single isolated QWW (see figure 3(b) in reference [31]): one (0–0) intrasubband magnetoplasmon branch ω_{mp}^{00}, but three (1–0) intersubband magnetoplasmon branches $\omega_{mp}^{10;1}$, $\omega_{mp}^{10;2}$, $\omega_{mp}^{10;3}$ and also three (2–0) intersubband magnetoplasmon branches $\omega_{mp}^{20;1}$, $\omega_{mp}^{20;2}$ and $\omega_{mp}^{20;3}$ are observable. Thus, we find for the magnetoplasmons of the LMWSL besides the *fundamental* (intersubband) *modes* (FMs), $\omega_{mp}^{N0;\,j=1}$, also the *additional* (intersubband) *modes* (AMs), $\omega_{mp}^{N0;\,j>1}$. Here, the quantum number j denotes the magnetoplasmon minibands of each group $\{N0\}$, ordered according to decreasing depolarization shift. Hence, the spectrum of magnetoplasmons of a LMWSL shows the same *fine-structure effects* as that of Q1D magnetoplasmons of a single isolated QWW. This result is obvious because in the framework of the tight-binding approximation (with and without tunnelling) the modes of each single isolated wire play an important role in forming the Coulomb-coupled modes of the LMWSL. It is seen from figures 3(b) and 3(c) that for a smaller superlattice period both types of mode, FMs and AMs, are accompanied by a miniband structure of the dispersion relation. The minibands of the AMs have for a given magnetic field two stop-points

$$q_{xs(0)}^{N0;\,j} = q_x(q_y = 0; B|\omega_{mp}^{N0;\,j} = \omega_1^{N0})$$

and

$$q_{xs(\pi/d)}^{N0;\,j} = q_x(q_y = \pi/d; B|\omega_{mp}^{N0;\,j} = \omega_1^{N0})$$

at the upper boundary ω_1^{N0} of the corresponding single-particle continuum. Hence, for $q_x > q_{xs(q_y)}^{N0;\,j}(q_y; B)$ the AMs become Landau damped. Further stop-points may occur for different parameters of the LMWSL at the boundaries of other SPE continua.

The RPA dispersion curves of the magnetoplasmons in the ω–B plane are plotted in figures 4(a) and 4(b) for $q_x = 0$ and two different periods d of the LMWSL, respectively. Again,

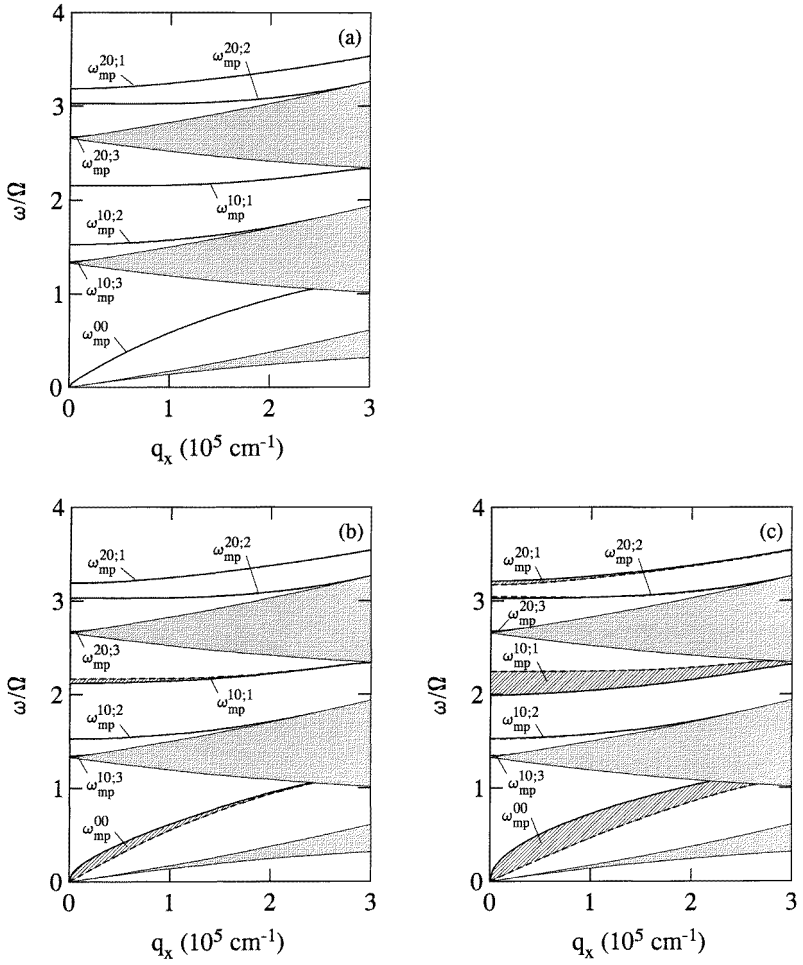

Figure 3. The dependence of the dispersion relations of the magnetoplasmons of a LMWSL calculated in the RPA on the wave-vector component q_x for $B = 1$ T: (a) $d = 1000$ nm, (b) $d = 200$ nm and (c) $d = 100$ nm. The hatched areas indicate the magnetoplasmon minibands (boundaries are shown for $q_y = 0$ by solid curves and for $q_y = \pi/d$ by dashed curves) and the shaded areas correspond to the single-particle intra- and intersubband continua.

these dispersion curves are plotted for the boundaries of the magnetoplasmon minibands: $\omega_{mp}^{N0;\,j}(q_y = 0)$ and $\omega_{mp}^{N0;\,j}(q_y = \pi/d)$. It is seen from these figures that for $q_x = 0$ the intrasubband magnetoplasmon ω_{mp}^{00} is absent and the SPE continua degenerate to the single lines $\tilde{\omega}_c$, $2\tilde{\omega}_c$, $3\tilde{\omega}_c, \ldots$, shown by the thin solid curves. That in the absence of electron tunnelling between the wires the intrasubband magnetoplasmon modes vanish for $q_x = 0$ becomes obvious from the fact that for $q_x = 0$ there is no electron motion along each wire. Thus, for $d \to \infty$, i.e. in the case of single isolated QWWs, no magnetoplasmons are present at $q_x = 0$ and these modes cannot be generated by the Coulomb coupling for decreasing d. It is seen that the widths of the intersubband magnetoplasmon minibands decrease with increasing magnetic field and the intersubband magnetoplasmons approach for large magnetic fields (i.e. in the 2D limit) multiples of the cyclotron frequency ω_c. Thus, the (1–0) intersubband magnetoplasmon branches $\omega_{mp}^{10;\,j}(q_x = 0, q_y; B)$ approach for large

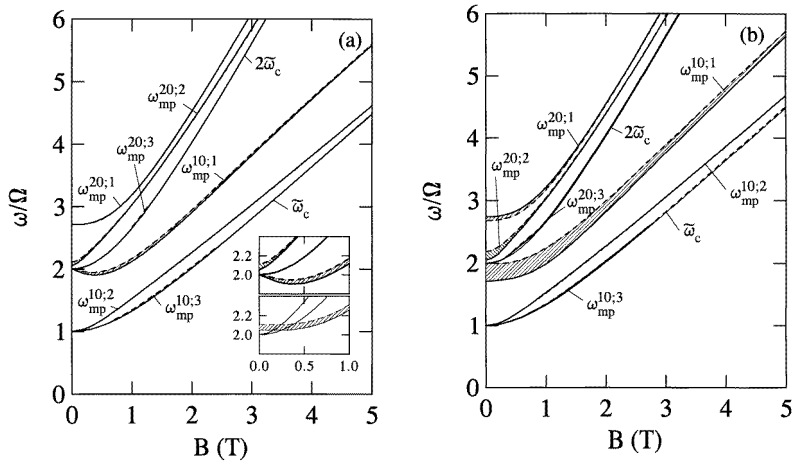

Figure 4. The dependence of the dispersion relations of the magnetoplasmons of a LMWSL calculated in the RPA on the magnetic field B for $q_x = 0$: (a) $d = 200$ nm and (b) $d = 100$ nm. The thin curves in the inset of (a) show the uncoupled modes, calculated using the diagonal approximation, and the heavy curves show the coupled modes. The hatched areas indicate the magnetoplasmon minibands (boundaries are shown for $q_y = 0$ by solid curves and for $q_y = \pi/d$ by dashed curves).

magnetic fields the dispersion curve of the *principal mode* of a 2DEG and the (2–0) intersubband magnetoplasmon branches $\omega_{mp}^{20;j}(q_x = 0, q_y; B)$ approach in this limit the dispersion relation of the first *Bernstein mode* of a 2DEG (see e.g. reference [48] for the magnetoplasmons of a 2DEG). It becomes obvious from figures 4(a) and 4(b) that the properties of the FM and AM minibands are different. The FM minibands have for all magnetic fields a finite depolarization shift, whereas in general the depolarization shift of the AM minibands vanishes at $B = 0$ and for $B \to \infty$. It is seen that in figures 4(a) and 4(b) the depolarization shift of the AM branches denoted by $\omega_{mp}^{10;2}$ and $\omega_{mp}^{10;3}$ vanishes at $B = 0$, but the AM branch denoted by $\omega_{mp}^{20;2}$ does not show this property. The reason for this different behaviour of the branch $\omega_{mp}^{20;2}$ is that the *uncoupled modes* $\omega_{mp}^{10;1}$ and $\omega_{mp}^{20;2}$ (i.e. the '*pure*' modes), which are calculated in the *diagonal approximation* by using

$$P_{NN'}^{(1)} = [\delta_{NN_1}\delta_{N'N_2}P_{N_1N_2}^{(1)} + \delta_{NN_2}\delta_{N'N_1}P_{N_2N_1}^{(1)}]/(1 + \delta_{N_1N_2})$$

in equation (25) (for details see reference [31]) and shown by the thin curves in the inset of figure 4(a), do cross at small magnetic fields. Such a crossing of the uncoupled modes becomes possible because the depolarization shift of the FMs increases with increasing electron density, while the AMs are pinned at the upper boundary of the associated SPE continuum at $B = 0$. If the accompanying electron transitions of the crossing branches are not independent, the ISC results in a mode hybridization, i.e. in two resonance-split hybrid modes. Thus, the branch denoted by $\omega_{mp}^{20;2}$ has for small magnetic fields (i.e. left from the crossing of the uncoupled modes) the character of the FM $\omega_{mp}^{10;1}$ and, hence, has a finite depolarization shift at $B = 0$. With increasing magnetic field the character of this branch becomes more and more that of an AM. The opposite is true for the branch denoted by $\omega_{mp}^{10;1}$. It is noticeable that, depending on the concrete set of physical parameters of the LMWSL, many such resonance splittings may occur. This results in a very complex mode spectrum with branches of dispersion curves showing quite different character when varying the magnetic field. Obviously, the depolarization shift of the AM minibands has its maximum at intermediate magnetic fields, where the magnetic

quantization becomes comparable with the size quantization in each wire. Hence, the FMs $\omega_{mp}^{N0;\,j=1}$ have the property $\omega_{mp}^{N0;1} \to \omega_{p}^{N0}$ if $B \to 0$ and they also exist for $B \to \infty$, whereas the ('pure') AMs $\omega_{mp}^{N0;\,j>1}$ are absent for $B = 0$ and $B = \infty$. As shown in reference [31], for $B \neq 0$ and $B \neq \infty$ the AMs of a single isolated QWW arise due to the reduced symmetry in the presence of a magnetic field. The FMs and AMs can be interpreted for larger magnetic fields (i.e. near the 2D limit) as *confined principal modes* ($\omega_{mp}^{10;\,j}$) and *confined Bernstein modes* ($\omega_{mp}^{N0;\,j}$ for each pair $\{N0\}$ with $N > 1$), which strongly hybridize at intermediate and smaller magnetic fields. Furthermore, for $B \to 0$ the FMs originate from the confined principal modes and the AMs lose their collective character at $B = 0$ like the Bernstein modes of a 2DEG or a 3DEG, i.e. in this limit the AMs may be interpreted as the Q1D analogues of the Bernstein modes. It should be noted that for very large magnetic fields all magnetoplasmon modes of the LMWSL are free of Landau damping because of the completely quantized situation in the 2D limit.

In figures 5(a) and 5(b) the corresponding collective excitations, i.e. the mixed (0–0)–(1–0)–(2–0) magnetoplasmons, are plotted for the finite-wave-vector component $q_x = 1 \times 10^5\ \mathrm{cm}^{-1}$. In this case the intrasubband magnetoplasmon miniband ω_{mp}^{00} is present and the SPE continua have a finite width. The intrasubband magnetoplasmon miniband shows for fixed q_x and q_y a negative slope with increasing magnetic field, i.e. the intrasubband magnetoplasmon branch of a LMWSL has the character of an *edge mode*, analogous to the intrasubband magnetoplasmon of a single isolated QWW. The finite width of the SPE continua restricts the regions of existence of the collective modes free of Landau damping. From figures 5(a) and 5(b) it becomes obvious that the AMs, $\omega_{mp}^{N0;\,j>1}$, approach for $B \to 0$ and $B \to \infty$ the corresponding single-particle continua. Thus, in the case of a finite wave vector of the modes we have at $B = 0$ the well-known picture of plasmons in a LMWSL (see e.g. reference [11]) and at $B = \infty$ that of 2D magnetoplasmons (see e.g. reference [48]). At large but finite magnetic fields we have the confined principal modes (FM and AMs) and the confined Bernstein modes (FMs and AMs). Like in the case of vanishing q_x, for $q_x \neq 0$

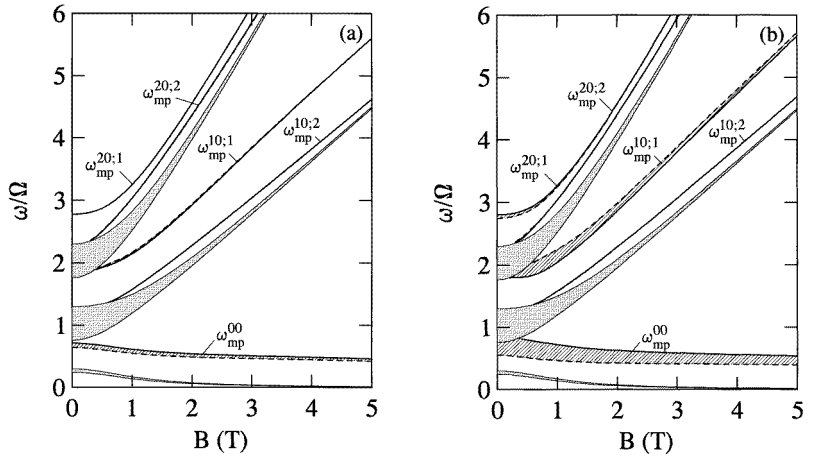

Figure 5. The dependence of the dispersion relations of the magnetoplasmons of a LMWSL calculated in the RPA on the magnetic field B for $q_x = 1 \times 10^5\ \mathrm{cm}^{-1}$: (a) $d = 200$ nm and (b) $d = 100$ nm. The hatched areas indicate the magnetoplasmon minibands (boundaries are shown for $q_y = 0$ by solid curves and for $q_y = \pi/d$ by dashed curves) and the shaded areas correspond to the single-particle intra- and intersubband continua.

and finite (intermediate) magnetic fields the different modes strongly hybridize and for small magnetic fields ($B \to 0$) the FMs originate from the confined principal modes and the AMs from the confined Bernstein modes. It is important to note that the *fine structure* of the intersubband magnetoplasmons of a LMWSL occurs independently of the shape of the lateral confining potential. Thus, the existence of FMs and AMs is just the consequence of the *reduced symmetry* and, therefore, a *fundamental* and *intrinsic property* due the Q1D quantization in each wire, and this property is conserved in the presence of Coulomb coupling between the different wires.

From the results discussed up to now, it becomes obvious why the theory of magnetoplasmons for single isolated QWWs, presented in reference [31], explains very well the experimental results [4, 36] obtained for LMWSLs. The theory developed here, valid for magnetoplasmons in LMWSLs, gives the same types of mode—intrasubband modes and two

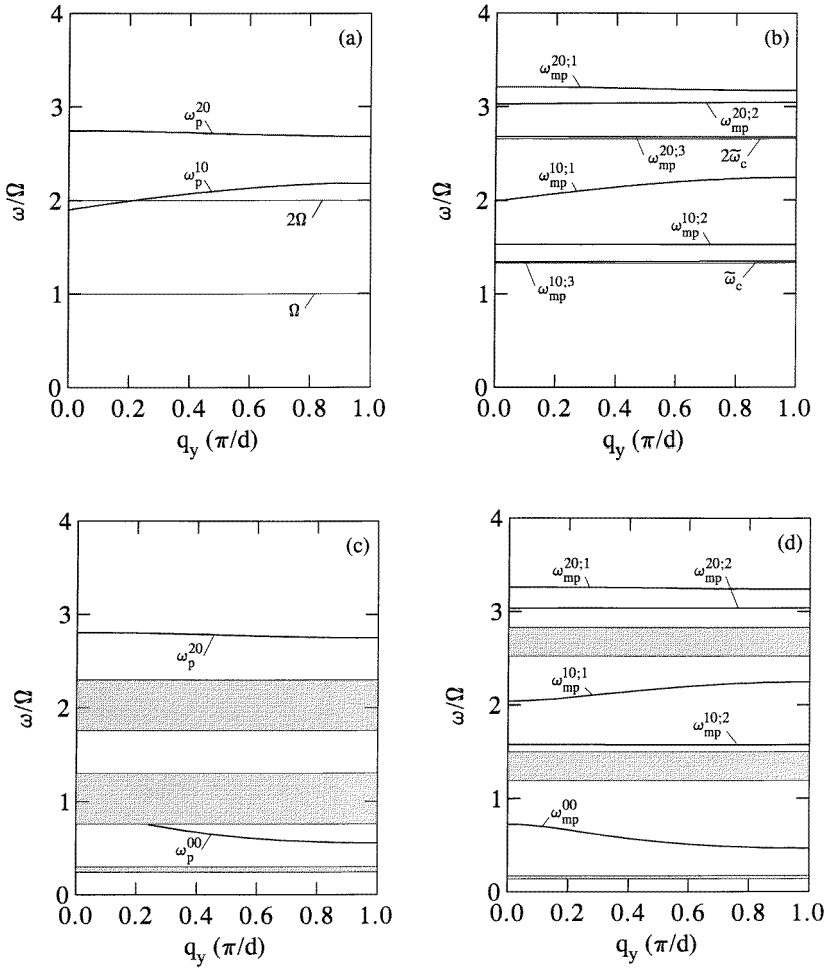

Figure 6. The dependence of the dispersion relations of the plasmons and magnetoplasmons of a LMWSL calculated in the RPA on the wave-vector component q_y for $d = 100$ nm: (a) $B = 0$, $q_x = 0$; (b) $B = 1$ T, $q_x = 0$; (c) $B = 0$, $q_x = 1 \times 10^5$ cm^{-1}; and (d) $B = 1$ T, $q_x = 1 \times 10^5$ cm^{-1}. The shaded areas correspond to the single-particle intra- and intersubband continua.

types of intersubband mode: FMs and AMs—as in the case of a single isolated QWW. Besides the additional dispersion according to the mode propagation along the y-axis, these modes have in both systems the same physical properties and, as shown above, the additional dispersion with q_y does not result in any mode crossing/anticrossing behaviour. Furthermore, because this dispersion only becomes important for superlattice periods $d < 200$ nm, the theory of magnetoplasmons for a single QWW and that for a LMWSL give for superlattice periods of $d \geqslant 350$ nm, as used in the experiments presented in references [4,36], the same results. Hence, the theory of magnetoplasmons in LMWSLs developed here is able to explain the experiments performed up to now and it should also be a powerful method for explaining further experiments on shorter-period LMWSLs including the case for which tunnelling between the wires becomes important.

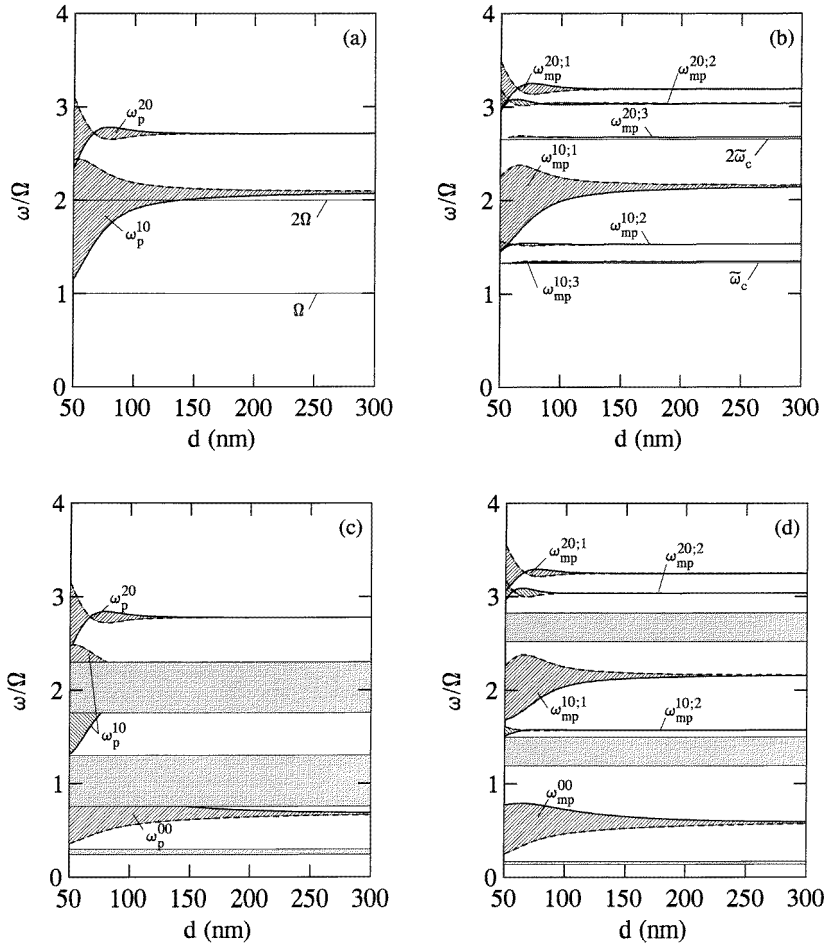

Figure 7. The dependence of the dispersion relations of the plasmons and magnetoplasmons of a LMWSL calculated in the RPA on the superlattice period d: (a) $B = 0$, $q_x = 0$; (b) $B = 1$ T, $q_x = 0$; (c) $B = 0$, $q_x = 1 \times 10^5$ cm^{-1}; and (d) $B = 1$ T, $q_x = 1 \times 10^5$ cm^{-1}. The hatched areas indicate the magnetoplasmon minibands (boundaries for $q_y = 0$ are shown by solid curves and for $q_y = \pi/d$ by dashed curves) and the shaded areas correspond to the single-particle intra- and intersubband continua.

The dependences of the RPA dispersion relations of the plasmons and magnetoplasmons of the LMWSL on the wave-vector component q_y are plotted in figures 6(a) to 6(d) for two different values of the wave-vector component q_x and two different values of the magnetic field B. It is seen that with increasing q_y the frequency of the intrasubband magnetoplasmon always decreases, while those of the intersubband magnetoplasmons behave differently. The strength and sign of the dispersion of a given intersubband mode depend on the superlattice period, as shown in figure 7.

In figures 7(a) to 7(d) the dependences of the dispersion relations of the plasmons and magnetoplasmons of the LMWSL on the superlattice period d are plotted for two different wave-vector components q_x and magnetic fields B. It is seen that with increasing d the widths of the minibands decrease. For $d \geqslant 300$ nm the miniband widths of the branches plotted is practically zero and the frequencies of the modes become independent of d, i.e. the Coulomb coupling becomes unimportant for the modes. Physically this means that for lateral distances larger than 300 nm the bare Coulomb potential becomes nearly totally screened. Thus, in this way, we have found that the *lateral screening length* $[q_y^s]^{-1}$ is about 200–250 nm for the LMWSL under consideration.

Please note that for $d < 100$ nm electron tunnelling between the single QWWs of the LMWSL may become important, leading in this range to deviations from the plotted plasmon and magnetoplasmon minibands.

The dependences of the RPA dispersion relations of the plasmons and magnetoplasmons of the LMWSL under consideration on the angle φ between the x-axis and the wave vector $\boldsymbol{q}_\parallel = (q_x, q_y)$ of the propagating mode in the x–y plane are plotted in figures 8(a) and 8(b): $q_x = q_\parallel \cos\varphi$, $q_y = q_\parallel \sin\varphi$, $q_\parallel = (q_x^2 + q_y^2)^{1/2}$. From figure 8(a) it is seen that in the case of $B = 0$ and $q_\parallel = 1 \times 10^5$ cm^{-1}, for small angles only the intersubband plasmon ω_p^{20} occurs as a collective mode, while the (0–0) intrasubband plasmon and the (1–0) intersubband plasmon are Landau damped. But for larger angles, the plasmon modes ω_p^{00} and ω_p^{10} also appear in the spectrum of the collective excitations. For $B = 1$ T (figure 8(b)) the modes ω_{mp}^{00}, $\omega_{mp}^{10;1}$, $\omega_{mp}^{10;2}$, $\omega_{mp}^{20;1}$ and $\omega_{mp}^{20;2}$ appear for $0 \leqslant \varphi \leqslant \pi/2$ and the modes $\omega_{mp}^{10;3}$ and $\omega_{mp}^{20;3}$ are resolvable from the upper boundary of the corresponding SPE continuum only for larger φ.

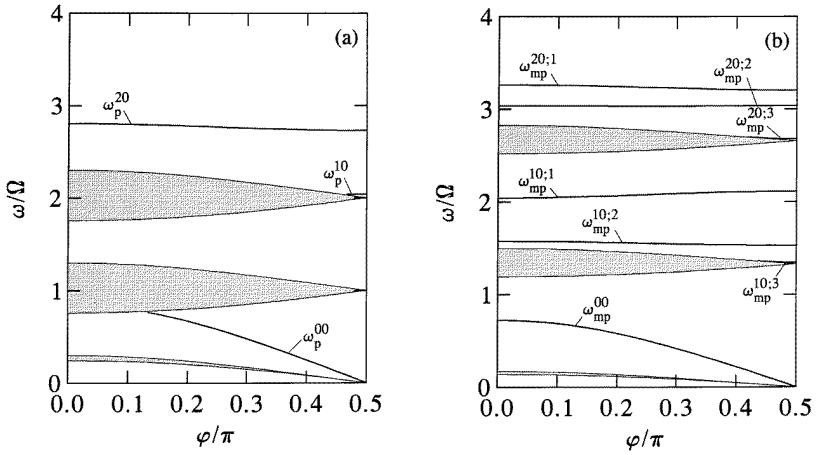

Figure 8. The dependence of the dispersion relations of the plasmons and magnetoplasmons of a LMWSL calculated in the RPA on the angle φ between the x-axis and the propagation direction of the mode in the x–y plane for $q_\parallel = 1 \times 10^5$ cm^{-1} and $d = 100$ nm: (a) $B = 0$ and (b) $B = 1$ T. The shaded areas correspond to the single-particle intra- and intersubband continua.

5. Conclusions

In this work, we have investigated the magnetoplasmons of a lateral multiwire superlattice using the tight-binding approximation for the electronic ground state to calculate the dynamical response. The magnetoplasmons of each wire are coupled via the Coulomb coupling forming the magnetoplasmons of the LMWSL which can propagate in the x–y plane. The theory developed here takes into account Umklapp processes. It is shown that the magnetoplasmons of LMWSLs show the same fine-structure effects as the magnetoplasmons of a single isolated QWW [31] and, thus, the normal modes of the system can be classified into fundamental and additional modes. According to a possible mode propagation perpendicular to the wire axes due to the Coulomb coupling, the mode spectrum shows minibands for both FMs and AMs. The FM minibands are defined as such minibands, which exist (i) at $B = 0$, where the modes forming the FM minibands become identical to the plasmons of the corresponding LMWSL, and (ii) at $B = \infty$, where these modes become the principal mode and the Bernstein modes of a two-dimensional electron gas. Between these limits the reduced symmetry causes fine-structure effects. Hence, the principal mode and the Bernstein modes of a 2DEG become split in a LMWSL with the result that the FM and AM minibands appear. The AM minibands approach for $B \to 0$ the associated frequencies of the single-particle excitation and, hence, lose their collective character. Thus, at small magnetic fields the AMs may be interpreted as the Bernstein modes of the LMWSL. For intermediate magnetic fields strong-hybridization effects appear in the mode spectrum. This picture of the magnetoplasmon spectrum for a LMWSL is independent of the shape of the lateral confining potential and, thus, is universal. As shown in reference [31], depending on the physical parameters of the single QWWs, many crossing/anticrossing effects can occur. But these effects have their origin in the mode spectrum of the Q1DEG in the single isolated wire alone. The Coulomb coupling between the magnetoplasmons of the different wires does not give rise to additional crossing/anticrossing effects in the mode spectrum.

Our theory is the first quantum theory of magnetoplasmons which agrees very well with that of plasmons in LMWSLs for $B = 0$ [11], with the 2D case for $B \to \infty$ [48] and shows the same fine-structure effects as a single isolated QWW [31] for finite magnetic fields, realizing this limit for $d \to \infty$. It is shown that the Coulomb coupling of the magnetoplasmons and the resulting miniband structure become important only for superlattice periods $d < 200$ nm. For larger-period LMWSLs the results for a LMWSL and for a single isolated QWW become practically the same. Thus, the theory developed here is successful in explaining recent experimental results, which were obtained for larger-period LMWSLs. Furthermore, this theory should be successful in explaining future experimental work on shorter-period LMWSLs including the case in which tunnelling between the wires becomes important.

Acknowledgments

The authors gratefully acknowledge financial support from the Deutsche Forschungsgemeinschaft (DFG), Project We 1532/3-2.

References

[1] Calleja J M, Goñi A R, Dennis B S, Weiner J S, Pinczuk A, Schmitt-Rink S, Pfeiffer L N, West K W, Müller J F and Ruckenstein A E 1991 *Solid State Commun.* **79** 911

[2] Plaut A S, Lage H, Grambow P, Heitmann D, von Klitzing K and Ploog K 1991 *Phys. Rev. Lett.* **67** 1642

[3] Goñi A R, Pinczuk A, Weiner J S, Calleja J M, Dennis B S, Pfeiffer L N and West K W 1991 *Phys. Rev. Lett.* **67** 3298
[4] Hertel G, Drexler H, Hansen W, Schmeller A, Kotthaus J P, Holland M and Beaumont S P 1994 *Solid State Electron.* **37** 1289
[5] Frank W R, Govorov A O, Kotthaus J P, Steinebach C, Gudmundsson V G, Hansen W and Holland M 1997 *Phys. Rev.* B **55** R1950
[6] Lee Y C, Ulloa S E and Lee P S 1983 *J. Phys. C: Solid State Phys.* **16** L995
[7] Tsukada M, Ishida H and Shima N 1984 *Phys. Rev. Lett.* **53** 376
[8] Das Sarma S and Lai W Y 1985 *Phys. Rev.* B **32** 1401
[9] Eliasson G, Wu J-W, Hawrylak P and Quinn J J 1986 *Solid State Commun.* **60** 41
[10] Cautadella V and Iadonisi G 1987 *Phys. Rev.* B **35** 7443
[11] Que W and Kirczenow G 1988 *Phys. Rev.* B **37** 7153
[12] Que W and Kirczenow G 1989 *Phys. Rev.* B **39** 5998
[13] Li Q P and Das Sarma S 1990 *Phys. Rev.* B **41** 10 268
[14] Mendoza B S and Schaich W L 1991 *Phys. Rev.* B **43** 9275
[15] Que W 1991 *Phys. Rev.* B **43** 7127
[16] Wendler L, Haupt R and Pechstedt R 1991 *Phys. Rev.* B **43** 14 669
[17] Hu G Y and O'Connell R F 1991 *Phys. Rev.* B **44** 3140
[18] Li Q P and Das Sarma S 1991 *Phys. Rev.* B **44** 6277
[19] Gumbs G, Huang D and Heitmann D 1991 *Phys. Rev.* B **44** 8084
[20] Haupt R, Wendler L and Pechstedt R 1991 *Phys. Rev.* B **44** 13 635
[21] Wendler L, Haupt R and Pechstedt R 1992 *Surf. Sci.* **263** 363
[22] Wendler L and Haupt R 1992 *Quantum Effect Physics, Electronics and Applications (IOP Conf. Proc. 127)* ed K Ismail, T Ikoma and H I Smith (Bristol: Institute of Physics Publishing) ch 2, p 51
[23] Wendler L and Haupt R 1992 *Proc. 21st Int. Conf. on The Physics of Semiconductors* ed Ping Jiang and Hon-Zhi Zheng (Singapore: World Scientific) p 1343
[24] Wendler L, Grigoryan V G and Haupt R 1992 *Superlatt. Microstruct.* **12** 501
[25] Wendler L and Grigoryan V G 1994 *Phys. Status Solidi* b **181** 133
[26] Wendler L and Grigoryan V G 1994 *Phys. Rev.* B **49** 13 607
[27] Wendler L and Grigoryan V G 1994 *Phys. Rev.* B **49** 14 531
[28] Wendler L and Haupt R 1995 *Phys. Rev.* B **52** 9031
[29] Wendler L and Grigoryan V G 1995 *Europhys. Lett.* **32** 7
[30] Wendler L and Grigoryan V G 1996 *Solid State Commun.* **98** 683
[31] Wendler L and Grigoryan V G 1996 *Phys. Rev.* B **54** 8652
[32] Hansen W, Horst M, Kotthaus J P, Merkt U, Sikorski Ch and Ploog K 1987 *Phys. Rev. Lett.* **58** 2586
[33] Demel T, Heitmann D, Grambow P and Ploog K 1988 *Phys. Rev.* B **38** 12 372
[34] Merkt U 1989 *Superlatt. Microstruct.* **6** 341
[35] Demel T, Heitmann D, Grambow P and Ploog K 1991 *Phys. Rev. Lett.* **66** 2657
[36] Drexler H, Hansen W, Kotthaus J P, Holland M and Beaumont S P 1992 *Phys. Rev.* B **46** 12 849
[37] Weiner J S, Danan G, Pinczuk A, Valladares J, Pfeiffer L N and West K W 1989 *Phys. Rev. Lett.* **63** 1641
[38] Egeler T, Abstreiter G, Weimann G, Demel T, Heitmann D, Grambow P and Schlapp W 1990 *Phys. Rev. Lett.* **65** 1804
[39] Goñi A R, Pinczuk A, Weiner J S, Dennis B S, Pfeiffer L N and West K W 1993 *Phys. Rev. Lett.* **70** 1151
[40] Schmeller A, Goñi A R, Pinczuk A, Weiner J S, Calleja J M, Dennis B S, Pfeiffer L N and West K W 1994 *Phys. Rev.* B **49** 14 778
[41] Strenz R, Roßkopf V, Hirler F, Abstreiter G, Böhm G, Tränkle G and Weimann G 1994 *Semicond. Sci. Technol.* **9** 399
[42] Dahl C, Jusserand B and Etienne B 1995 *Phys. Rev.* B **51** 17 211
[43] Steinebach C, Krahne R, Biese G, Schüller C, Heitmann D and Eberl K 1996 *Phys. Rev.* B **54** R14 281
[44] Schüller C, Biese G, Keller K, Steinebach C, Heitmann D, Grambow P and Eberl K 1996 *Phys. Rev.* B **54** R17 304
[45] Wendler L and Grigoryan V G 1998 *Physica* B **245** 127
[46] Laux S E and Stern F 1986 *Appl. Phys. Lett.* **49** 91
[47] Laux S E, Frank D J and Stern F 1988 *Surf. Sci.* **196** 101
[48] Wendler L and Pechstedt R 1990 *J. Phys.: Condens. Matter* **2** 8881